AIP | The Journal of Chemical Physics

Metadynamics simulations of calcite crystallization on self-assembled monolayers

D. Quigley, P. M. Rodger, C. L. Freeman, J. H. Harding, and D. M. Duffy

Citation: The Journal of Chemical Physics **131**, 094703 (2009); doi: 10.1063/1.3212092
View online: http://dx.doi.org/10.1063/1.3212092
View Table of Contents: http://scitation.aip.org/content/aip/journal/jcp/131/9?ver=pdfcov
Published by the AIP Publishing

Articles you may be interested in

A molecular simulation study of an organosilane self-assembled monolayer/ Si O 2 substrate interface
J. Chem. Phys. **128**, 164710 (2008); 10.1063/1.2895052

Molecular simulation studies of the structure of phosphorylcholine self-assembled monolayers
J. Chem. Phys. **125**, 174714 (2006); 10.1063/1.2363978

Electric field induced switching of poly(ethylene glycol) terminated self-assembled monolayers: A parallel molecular dynamics simulation
J. Chem. Phys. **121**, 5427 (2004); 10.1063/1.1781120

Surface vibrations in alkanethiol self-assembled monolayers of varying chain length
J. Chem. Phys. **120**, 3880 (2004); 10.1063/1.1643353

Erratum: “In situ studies of thiol self-assembly on gold from solution using atomic force microscopy” [J. Chem. Phys. 108, 5002 (1998)]
J. Chem. Phys. **113**, 9357 (2000); 10.1063/1.1320001

This article is copyrighted as indicated in the article. Reuse of AIP content is subject to the terms at: http://scitation.aip.org/termsconditions. Downloaded to IP: 144.82.108.120 On: Fri, 03 Jul 2015 13:35:29

Metadynamics simulations of calcite crystallization on self-assembled monolayers

D. Quigley,[1,a)] P. M. Rodger,[1] C. L. Freeman,[2] J. H. Harding,[2] and D. M. Duffy[3]
[1]*Department of Chemistry and Centre for Scientific Computing, University of Warwick, Gibbet Hill Road, Coventry CV4 7AL, United Kingdom*
[2]*Department of Engineering Materials, University of Sheffield, Sir Robert Hadfield Building, Mappin Street, Sheffield S1 3JD, United Kingdom*
[3]*Department of Physics and Astronomy, University College London, Gower Street, London WC1E 6BT, United Kingdom*

(Received 29 June 2009; accepted 3 August 2009; published online 3 September 2009)

We show that recent developments in the application of metadynamics methods to direct simulations of crystallization make it possible to predict the orientation of crystals grown on self-assembled monolayers. In contrast to previous studies, the method allows for dynamic treatment of the organic component and the inclusion of explicit surface water without the need for computationally intensive interfacial energy calculations or prior knowledge of the interfacial structure. The method is applied to calcite crystallization on carboxylate terminated alkanethiols arrayed on Au (111). We demonstrate that a dynamic treatment of the monolayer is sufficient to reproduce the experimental results without the need to impose epitaxial constraints on the system. We also observe an odd-even effect in the variation of selectivity with organic chain length, reproducing experimentally observed orientations in both cases. Analysis of the ordering process in our simulations suggests a cycle of mutual control in which both the organic and mineral components induce complementary local order across the interface, leading to the formation of a critical crystalline region. The influence of *p*H, together with some factors that might affect the range of applicability of our method, is discussed. © *2009 American Institute of Physics*. [doi:10.1063/1.3212092]

I. INTRODUCTION

Biomineralization is the process by which living organisms manufacture bioceramic composite material such as shell, teeth, and bone. A remarkable level of control is exerted over crystalline morphology and orientation to create complex structures with intricate features over a range of length scales. There is considerable value in reproducing these biological processes as a means of manufacturing advanced materials.

Mineral growth on substrates functionalized with an organic self-assembled monolayer (SAM) has attracted interest as one such biomimetic process. Depending on the choice of chain length, head group, and ionization state, crystals on these substrates can be preferentially grown in a particular orientation. The solution chemistry of the growth medium also plays a role, interacting with both the mineral and the organic substrate to select particular polymorphs and growth morphologies (e.g., Refs. 1 and 2). A wide range of systems have been studied experimentally and we refer the reader to a recent review by Sommerdijk[3] in this area.

In principle, computer modeling can play a complementary role to these experimental studies. While difficult to access experimentally, the early (nucleation) stages of crystallization are ideally suited to the length scale of an atomistic computer simulation. Furthermore, many quantities which cannot be controlled in the laboratory can be specified exactly during *in silico* experiments, allowing factors such as monolayer flexibility to be introduced as variables.

In practice, predicting the crystallographic orientation which will arise from growth on a specific monolayer is a nontrivial modeling exercise. For example, mineral-substrate interfacial energy calculations are able to rank a series of candidate configurations and inform models based on classical nucleation theory.[4] Unfortunately the experimentally observed orientation is not guaranteed to be the thermodynamically stable state and may be selected by kinetic rather than purely thermodynamic considerations. Furthermore, the candidate configurations must be generated using information from experiments or epitaxial considerations, thus limiting the utility of such a model as a predictive tool.

There is considerable value in performing direct simulations of crystallization at the SAM, particularly in cases where simple epitaxial arguments fail to predict the nucleation plane. In simulations of this kind the preferred nucleation plane (and hence crystal orientation) should emerge naturally. It is this approach which we pursue in our present work, applied to the crystallization of calcium carbonate. Recent evidence from several monolayer experiments[5,6] and from simulation[7] has suggested that amorphous calcium carbonate (ACC) may be a precursor to the more stable calcite polymorph. The presence of an ACC precursor can overcome many of the solution chemistry constraints expected of a system obeying classical nucleation theory by ensuring a high local density of ions. Under these circumstances, a com-

[a)]Electronic mail: d.quigley@warwick.ac.uk.

 © 2009 American Institute of Physics

This article is copyrighted as indicated in the article. Reuse of AIP content is subject to the terms at: http://scitation.aip.org/termsconditions. Downloaded to IP: 144.82.108.120 On: Fri, 03 Jul 2015 13:35:29

putational study of crystal growth reduces to simulating crystallization of ACC deposits at the organic substrate and analyzing the resulting crystal.

Direct simulations of crystallization are, however, far from routine due to the long time scale associated with formation of a critical nucleus from which crystalline order can spread. The cost of forming an interface between crystalline and amorphous regions competes with the energetic preference for crystalline order resulting in a large energy barrier to crystal growth. Previous simulations of calcite growth on SAMs have employed elevated temperatures of 500 and 800 K to overcome this barrier.[8,9] This has proven highly effective in generating crystallized configurations on arrays of frozen carboxylic acid head groups. The use of such elevated temperatures, however, prohibits the inclusion of explicit solvent or dynamic treatment of the organic monolayer, two potentially important factors in reproducing experimental data.

In this paper we show that recent developments in the application of metadynamics to crystallization provide a powerful tool for overcoming this limitation. We apply this tool to crystallization of calcite on carboxylate terminated alkanethiol arrays on the gold (111) surface. Specifically we study monolayers of 16-mercaptohexadecanioc acid (MHA) and 15-mercaptopentadecanoic acid (MPA). These systems have been subjected to a range of both experimental and simulation studies, and so provide a suitable test bed for the method. We stress that the simulation methodology is directly applicable to crystallization on *any* SAM for which a computational model can be constructed.

Early experiments of crystallization on MHA monolayers demonstrated a preference for $(01\bar{1}5)$ as the nucleation plane.[10] In contrast, other experiments have demonstrated that this is the minority product and that the dominant nucleation plane is $(01\bar{1}2)$,[11,12] the disparity being attributed to a difference in *p*H in the starting solution. Interestingly, the dominant surface in the Bravais-Friedel-Donnay-Harker[13] morphology of calcite is the $(01\bar{1}2)$, as this direction has the largest interplanar spacing. This indicates that this surface is preferred provided the substrate can compensate for the surface charge density.

Han and Aizenberg[14] have suggested that the orientational specificity of alkanethiols on gold is rather poor, allowing for deviations of ± 10–$15°$ in the head group orientations and hence nucleation at the $(01\bar{1}l)$ plane where $l=2-5$. In contrast the orientational specificity on silver is tighter, consistently leading to nucleation at the $(01\bar{1}2)$ plane only. These authors also investigated odd chain lengths, including MPA on gold, and found they lead to a mixture of crystal orientations nucleated at the $(11\bar{2}0)$, $(11\bar{2}3)$, and $(11\bar{2}6)$ calcite planes. This odd-even effect was noticeably absent from simulations on silver substrates.

Experiments[12] and simple models for the MHA-calcite interface indicate a high degree of epitaxy between the $(01\bar{1}2)$ calcite surface and SAM, along the [100] calcite surface direction only. This suggests that line defects across the perpendicular direction are required to select these orientations. Furthermore, Duffy and Harding[15] have argued that rows of missing Ca^{2+} ions (as generated at the interface by this defect) are required to cancel the surface dipole moment of the charge mismatch. Surface energy calculations on these systems have demonstrated that defects of this kind can be generated by the inclusion of bicarbonate ions at the SAM and are sufficient to favor the experimentally observed $(01\bar{1}2)$ calcite surface at the interface. In the absence of these defects, the (0001) surface is preferred due to a higher degree of epitaxy with the ideal SAM. Modeling with flexible SAMs permits the formation of local density variations, which could eliminate the need for defects. Similarly, the effect of orientational specificity requires a dynamic treatment of the monolayer and may lead to nucleation at different crystallographic planes to the ideal case. The metadynamics method allows for this by biasing order parameters *local* to the calcium carbonate deposit. The water layer and alkanethiol acid chains can therefore be included dynamically at appropriate biological temperatures via coupling of the entire system to a heat bath.

The remainder of this paper is organized as follows. In Sec. II we describe the model employed to simulate the SAM-calcite system and the application of metadynamics to this problem. In Sec. III we describe three analysis tools from which we can calculate the quantity of crystallized material, the orientation of the calcite crystal, and the epitaxial match between the mineral and the monolayer head groups. In Sec. IV we present results for a series of 16 crystallization simulations investigating the influence of SAM flexibility, head group ionization, chain length, and the presence of bicarbonate ions. Conclusions drawn from these simulations are presented in Sec. V.

II. SIMULATION METHODS

Construction of the simulations presented below requires reliable force-field models for the mineral, the organic monolayer, and interactions between the two. The system must also be initialized in a representative configuration in order for the metadynamics trajectories to be meaningful. Various assumptions must be made in interpreting these trajectories which are also discussed in this section.

A. Model system

We have employed models consistent with those employed in a previous study.[16] Calcium carbonate was modeled with the rigid-ion version of the Pavese force field[17,18] and water was modeled with the TIP3P potential.[19] The organic monolayer was represented with the CHARMM united atom force field,[20,21] consistent with previous simulations on these systems.[4,22,23]

Potentials for interaction between the mineral and organic components are somewhat less standard. Using the regular mixing rules does not account for the large charge disparity between the mineral and organic components. This underestimates repulsive terms leading to unreliable simulations. The organic-mineral potentials are therefore fitted us-

This article is copyrighted as indicated in the article. Reuse of AIP content is subject to the terms at: http://scitation.aip.org/termsconditions. Downloaded to IP: 144.82.108.120 On: Fri, 03 Jul 2015 13:35:29

TABLE I. List of potentials derived for the simulations described in this paper. Further potentials can be found elsewhere (Ref. 16).

		Buckingham potentials ($A\exp(-\rho/r)-C/r^6$)		
		A (kJ mol^{-1})	ρ (Å)	C (eV Å^{-6})
Ca	O[a]	104 684.1	0.297	0.0
		Lennard-Jones 12–6 potentials ($E_0[(R_0/r)^{12}-2(R_0/r)^6]$)		
		E_0 (kJ mol^{-1})	R_0 (Å)	
OC[b]	O[a]	0.0894	3.987	

[a]O refers to the carboxylic oxygen of the head group.
[b]OC refers to the carbonate oxygen in the calcite.

ing a known crystal with a charge interaction mimicking that of our actual system (see Ref. 16 for further details). The values can be seen in Table I.

All simulations were conducted using the DL_POLY (Ref. 24) simulation package, version 2.16, modified to include the metadynamics functionality described below.

B. Simulation geometry

Previous simulations on frozen arrays of carboxylic acid head groups have employed spherical ACC particles containing 116 units of calcium carbonate. These were initialized at or near the monolayer surface in vacuum. Initial metadynamics calculations on systems of this size resulted in crystallization to calcite only in the case where head groups were highly ionized. In other simulations the particle formed a vaterite-like rod spanning the periodic boundaries. In this work we have chosen to begin with a slab of ACC, initialized in contact with the organic head groups and periodic in the x and y directions. This bypasses the process by which the ACC wets the interface, which is not accelerated by the metadynamics and is substantially slower in water than in vacuum. Furthermore, we used larger deposits of 300 formula units. This allowed several layers of calcite to form at full coverage, making numerical identification of the crystal orientation substantially more accurate. Our simulations therefore correspond to a large nanoparticle of metastable ACC crystallizing directly to calcite upon contact with the SAM. An alternative mechanism (which we have not modeled here) involves crystallization to vaterite of smaller ACC nanoparticles, before growth and subsequent recrystallization to calcite.[5]

The configuration of the SAMs was taken from previous work.[22] Monolayers of both MHA and MPA have been used to investigate the odd-even effect. For each chain length we constructed a range of simulations which differed in the number of ionized carboxylic acid head groups. These were taken as non-ionized, half-ionized, or totally ionized. In the totally ionized case we included simulations both with and without the presence of bicarbonate ions, making a total of four simulations for each of the two chain lengths. Note that bicarbonate ions were initially located in the same fashion as in previous work,[22] but were free to migrate as the simulation progressed. Carbon and oxygen atoms associated with the bicarbonate were included in the computation of order parameters for metadynamics (see below). Excess calcium ions were added to maintain overall charge neutrality where necessary.

The slab of ACC was constructed from a supercell of aragonite by removing the periodic boundary conditions in the z direction only and heating to 3000 K. This was then relaxed onto each of the eight SAM configurations with 0.2 ns simulations at 310 K while holding the organic chains frozen. We have mapped the phase diagram of the present calcite model and confirmed that calcite is the stable crystal phase under these conditions.[25]

The head space above the ACC slab was then filled with a water film of sufficient thickness to represent the layers of ordered molecules expected to form at the $(10\bar{1}4)$ calcite surface. This corresponds to 480 water molecules in the present geometry. Each geometry has been simulated with both a frozen SAM and with all degrees of freedom in the monolayer treated dynamically. Coupling to a heat bath was accomplished using the Nosé–Hoover thermostat[26] with a relaxation time of 20 ps. This results in a total of 16 simulations which are summarized in Table III.

C. Metadynamics

Metadynamics[27] is an increasingly popular tool for accelerating the sampling of rare events. Recent work has made significant progress toward routine application of this method to the sampling of crystallization. Our implementation of the metadynamics method is described in detail in Ref. 28 and briefly summarized below for convenience. A more general description of the method has recently been presented by Laio and Gervasio.[29]

The metadynamics method accelerates rare events by characterizing a system in terms of one or more collective variables $s(\mathbf{r}^N)$ (functions of the $3N$ atomic coordinates) which distinguish between the states of interest and are capable of describing, in a collective sense, pathways which connect these states. In the direct variant of metadynamics (which we employ here), the collective variables are subjected to a history-dependent bias potential which encourages the dynamics to explore new regions of configuration space. In practice, this bias is constructed via the periodic deposition of repulsive Gaussian potentials centered on the current values of the collective variables $\mathbf{s}(\mathbf{r}^N)$,

TABLE II. Parameters used in computing the five Steinhardt order parameters used as metadynamics collective variables.

α	β	N_c	r_1 (Å)	r_2 (Å)
Ca	Ca	12	5.25	5.65
Ca	C	12	3.65	4.05
Ca	O	12	2.65	3.05
C	C	8	5.15	5.50
C	O	3	1.30	1.55

This article is copyrighted as indicated in the article. Reuse of AIP content is subject to the terms at: http://scitation.aip.org/termsconditions. Downloaded to IP: 144.82.108.120 On: Fri, 03 Jul 2015 13:35:29

TABLE III. Summary of the 16 metadynamics simulations. The percentage of bulk crystalline material is computed from a 2 ns standard equilibrium MD simulation using the final configuration generated by the metadynamics. In each case the crystal is oriented perpendicular to the indicated crystallographic plane. The outcome of surface vector analysis is shown only when unambiguous.

Index	Chain type	Chain treatment	% ionization	Bicarbonate	% bulk crystal	Surface vectors	Dominant angle (deg)	Orientation
1	MHA	Frozen	100	Yes	43.46	$01\bar{1}2$	60	$01\bar{1}2$
2	MHA	Frozen	100	No	54.44	0001	0	0001
3	MHA	Frozen	50	No	13.21	⋯	67	N/A[a]
4	MHA	Frozen	0	No	24.71	⋯	48	N/A[a]
5	MPA	Frozen	100	Yes	24.15	$11\bar{2}6$	0	0001
6	MPA	Frozen	100	No	68.22	0001	0	0001
7	MPA	Frozen	50	No	4.90	0001	0	0001[b]
8	MPA	Frozen	0	No	39.42	$10\bar{1}4$	45	$10\bar{1}4$
9	MHA	Free	100	Yes	35.58	⋯	64	$01\bar{1}2$
10	MHA	Free	100	No	44.90	⋯	67	$01\bar{1}2$
11	MHA	Free	50	No	49.68	$10\bar{1}4/01\bar{1}5$	28	Unclear[c]
12	MHA	Free	0	No	34.17	$01\bar{1}5$	28	Unclear[c]
13	MPA	Free	100	Yes	55.55	⋯	48	$11\bar{2}6$
14	MPA	Free	100	No	42.67	⋯	0	Mixed[d]
15	MPA	Free	50	No	5.55	⋯	0	N/A[a]
16	MPA	Free	0	No	63.12	$10\bar{1}4$	45	$10\bar{1}4$

[a]Insufficient crystalline material to analyze.
[b]Only crystalline at the interface.
[c]Cannot be matched to any surface in our reference database.
[d]Resembles gain boundary between two differently orientated crystals.

$$V[\mathbf{s}(\mathbf{r}^N),t] = w\sum_{k=1}^{N_G} \exp\left[\frac{-|\mathbf{s}(k\tau_G)-\mathbf{s}(t)|^2}{2\delta h^2}\right], \tag{1}$$

where w is the height of the Gaussians, δh is their width, and the sum runs over all N_G augmentations previously deposited at an interval of τ_G.

As the simulation progresses, energy barriers will become eventually accessible at normal temperatures, and the trajectory will escape from the initial free energy basin to locate alternative states.

In the current context, we employed Steinhardt order parameters (commonly employed in crystallization studies) computed for each of five different types of atom pairs as these collective variables. Specifically we computed order parameters from Ca–Ca, Ca–C, Ca–O, C–C, C–O separation vectors,

$$Q_l^{\alpha\beta} = \left[\frac{4\pi}{2l+1}\sum_{m=-l}^{l}\left|\frac{1}{N_c N_\alpha}\bar{Q}_{lm}^{\alpha\beta}\right|^2\right]^{1/2}, \tag{2}$$

where

$$\bar{Q}_{lm}^{\alpha\beta} = \sum_{b=1}^{N_b} f_c(r_b)Y_{lm}(\theta_b,\phi_b). \tag{3}$$

The index b runs over all N_b bonds of length r_b between atoms of type α and β. Values for N_c, r_1, and r_2 are given in Table II. N_α is set to the total number of atoms present which belong to species α. Contributions to Eq. (3) are restricted to short range by the tapering function $f_c(r)$ which decays to zero between r_1 and r_2. Further details on the computation of these order parameters can be found in another paper.[28]

We also employed a sixth order parameter, the contribution to the potential energy from all real-space terms involving a calcium or carbonate/bicarbonate ion. In the case of long range electrostatic terms (which are treated in our work by the Ewald method), the reciprocal space terms are not as easily partitioned, hence are excluded from this order parameter. As in previous work we scaled each order parameter by a constant prefactor such that fluctuations in each are approximately equal at equilibrium. This optimizes the filling of the initial free energy basin and hence the rate at which new energy basins are found.

The inclusion of Steinhardt order parameters in the metadynamics introduces forces which are spatially complex and require a reduced simulation timestep to integrate accurately. All simulations reported in this paper use a timestep of 0.5 fs for this reason.

In the current context, we do not aim to produce a free energy map as a function of these order parameters. Obtaining such a map to suitable accuracy would require considerably longer simulations than those we report here. Rather we employ metadynamics purely as a means to generate crystallization trajectories. In interpreting these trajectories we have made the following assumptions.

(1) The trajectory will escape the initial free energy minimum by following the lowest free energy pathway.
(2) The bias potential does not dominate over the influence of the SAM, and hence crystallization will occur via heterogeneous nucleation at the interface.
(3) The crystal growth along this pathway will be therefore represent that preferentially selected by the presence of the SAM.

This article is copyrighted as indicated in the article. Reuse of AIP content is subject to the terms at: http://scitation.aip.org/termsconditions. Downloaded to IP: 144.82.108.120 On: Fri, 03 Jul 2015 13:35:29

The crystallized configurations will hence correspond to the energetically preferred crystal orientation on the monolayer. The second assumption is simple to validate by tracking the emergence of local order during each simulation. The first assumption is harder to justify. Metadynamics simulations are not guaranteed to locate the lowest free energy pathway. If the bias potential is not grown carefully, substantial overfilling of the initial basin can occur leading to escape via higher energy pathways. We have therefore ensured that the bias potential is grown sufficiently slowly to avoid this problem. A poor choice of collective variables can also lead to identification of unphysical mechanisms.

D. Validation

To choose an appropriate Gaussian deposition rate for our simulations we refer to calculations of interfacial surface energies for calcite. Experimentally the $(10\bar{1}4)$ surface dominates both the equilibrium and growth morphology of calcite crystals. Calculations[30] have confirmed that this surface possesses the lowest energy by 0.38 J m^{-2} in vacuum and by 0.52 J m^{-2} in water. However, surface energy differences between the different faces of calcite grown on stearic acid monolayers are substantially lower,[31] ranging from approximately 0.05 to 0.1 J m^{-2}. Applying the lowest of these values to our current slab at 300 K, this defines an energy scale appropriate to the current problem of $\approx 140\ k_B T$. To minimize the risk of overfilling we used a Gaussian height of 2.5% of this value for each addition of the bias potential 1.

To determine a suitable deposition rate we have simulated crystallization of ACC slabs in vacuum. Four independent starting configurations were constructed by minimizing the energy of configurations obtained from a short trajectory of molten calcite at 3000 K. Each of the resulting simulation cells was then expanded by 100 Å in the z direction to generate a pseudo-two-dimensional periodic slab geometry. Applying the metadynamics to these systems provides an additional means to test the key assumptions of this work. In vacuum the lowest energy surface of calcite is known to be the nonpolar $(10\bar{1}4)$.[30] We therefore expect each of these slabs to crystallize with the $(10\bar{1}4)$ surface exposed. Simulations were performed at 300 K and at constant density. Gaussian deposition intervals of 0.25, 0.2, 0.15, and 0.05 ps were employed in four independent metadynamics simulations. Each simulation was terminated following the first crystallization event. The resulting configurations are shown in Fig. 1.

Regardless of deposition rate, the $(10\bar{1}4)$ is exposed in the resulting crystal. As stated above, the energy differences between the surfaces of interest when in contact with the monolayer are somewhat smaller than in the vacuum case. We have therefore adopted the longest deposition interval of 0.25 ps in the simulations which follow.

III. ANALYSIS

Three primary methods were employed to analyze the crystals generated. The first computed the fraction of calcium and carbonate ions that possessed local bond orientational order parameters that were a statistical match to those in bulk calcite. In this way the percentage of crystallized material could be computed at each simulation snapshot, providing confirmation of the polymorph selected and a single scalar variable which quantified the degree of crystallization. The second method used the orientation of carbonate ions relative to the surface normal to identify the crystallographic orientation of the calcite layer. The third method examined the positioning of the calcium ions at the monolayer-crystal interface and matched this to known calcite surfaces.

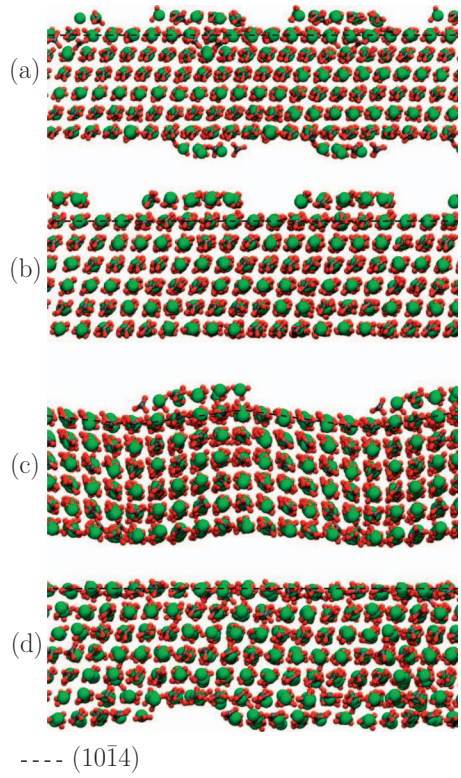

FIG. 1. Final crystallized configurations of calcium carbonate slabs in vacuum. The 1500 $CaCO_3$ unit cell has been replicated in the x-y plane for clarity. Crystallization was accelerated by applying the metadynamics scheme with Gaussian deposition intervals of (a) 0.25 ps, (b) 0.2 ps, (c) 0.15 ps, and (d) 0.05 ps. In each case planes belonging to $\{10\bar{1}4\}$ are exposed to vacuum. Islands and/or kinks in the surface are required to maintain the periodicity enforced by the simulation cell.

The constantly changing nature of the metadynamics trajectories is unsuitable for extracting statistical data on the equilibrium crystal. We therefore extracted the final crystallized configuration from each simulation and used it to initiate a standard molecular dynamics (MD) simulation for 2 ns. The analysis methods described below were applied to this relaxed trajectory.

A. Local order analysis

This analysis computes a number of order parameters to describe the local bonding environment around each ion. This can be compared to that in bulk calcite and used to quantify the fraction of material which has crystallized. The local order parameters are similar to the bulk Steinhardt order parameters biased by the metadynamics, but are com-

This article is copyrighted as indicated in the article. Reuse of AIP content is subject to the terms at: http://scitation.aip.org/termsconditions. Downloaded to IP: 144.82.108.120 On: Fri, 03 Jul 2015 13:35:29

puted on a per-ion basis including contributions from neighboring ions within a coordination radius. In the general case the local order parameter is defined as

$$q_l^{\alpha\beta} = \left[\frac{4\pi}{2l+1} \sum_{m=-l}^{l} \left| \frac{1}{N_{\alpha\beta}} \sum_{i=1}^{N_{\alpha\beta}} Y_{lm}(\theta_i, \phi_i) \right|^2 \right]^{1/2} \quad (4)$$

due to ions of type β in the coordination shell of an ion of type α. For calcium ions ($\alpha=1$) we computed three order parameters ($\beta=1$, 2, or 3) using calcium, carbon, and oxygen neighbors, respectively. For carbonate carbon atoms ($\alpha=2$) we computed two order parameters ($\beta=1$ or 2). A third carbonate order parameter was computed on the carbonate oxygens ($\alpha=3$) using calcium ion neighbor ($\beta=1$) contributions from all three oxygens present. Further details on the computation of these order parameters can be found in another paper.[28]

The instantaneous local order parameters for each ion type were then determined over a 125 ps simulation of bulk calcite at the temperature and pressure of interest. A covariance matrix for each set of three order parameters was constructed and diagonalized to yield linearly independent combinations of order parameters.

At each snapshot in a simulation trajectory we then computed (for each ion) the same linear combination of order parameters and compared to the reference bulk simulation. If the resulting values were within 3.5 standard deviations of each reference average, then we tagged the ion as belonging to a calcite-like local bonding environment. Note that in contrast to the data sets employed in other work,[28] we did not include covariance data for ideal surfaces due to overlap in the order parameter distributions between the many calcite surfaces of interest. The percentage of crystallized material computed from this method does not therefore include contributions from undercoordinated ions at the surface of the crystal, and so cannot approach 100%.

B. Orientational analysis

The angles adopted by carbonate anions within the mineral provide information on both the ordering of ions and orientation of the overall crystal. We calculated the orientation of each carbonate ion in relation to the *xy* plane of the cell (i.e., an angle of 0°/180° indicates the carbonate was parallel to the SAM surface). The orientation was calculated for all carbonates over the 2 ns simulation. From this data we were able to extract the angular frequency distribution of the carbonate groups. To remove background noise, these were constructed with respect to that of the ACC with no SAM present.

C. Surface vector analysis

Each calcite plane can be associated with a characteristic set of cation surface vectors. We have therefore compared the cation arrangements at the calcite-SAM interface to a number of ideal crystal surfaces using an epitaxial order parameter dependent on the local atomic environment. We first define a set of N_q two-dimensional wavevectors $\{\mathbf{q}_i\}$ which connect surface atom i to all N_z surface neighbors within a set cutoff r_c. This cutoff was chosen to lie between the second and third nearest neighbor distances of the three-dimensional Ca^{2+} sublattice. Note that we define *surface* vectors/atoms by restricting computation to ions within one repeat unit cell of the organic-mineral interface.

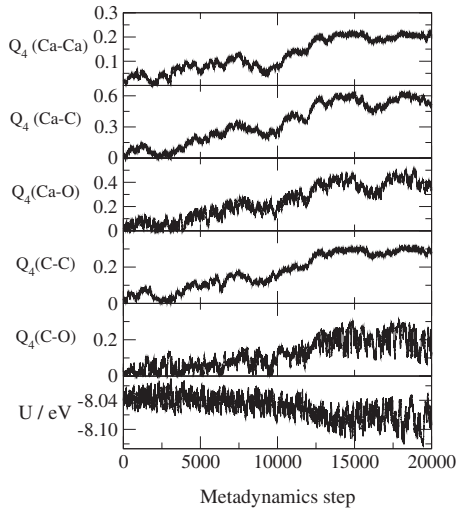

FIG. 2. Evolution of the six metadynamics collective variables during a typical crystallization simulation, in this case simulation 9 in Table III. The potential energy U is expressed per atom in the calcium carbonate layer.

When compared to a reference surface vector r,

$$\exp(i\mathbf{q}\cdot\mathbf{r}) = 1, \quad (5)$$

for a perfect match. A figure of merit for the match between the current surface vectors and a set of reference surface vectors is therefore

$$\Psi_i = \left[\frac{1}{N_q} \frac{1}{N_Z} \sum_{\mathbf{r}} \sum_{\mathbf{q}} \exp(i\mathbf{q}\cdot\mathbf{r}) \right]^2, \quad (6)$$

which we take as our local epitaxial order parameter.[32] This was computed for a number of reference surfaces constructed by minimizing the energy of a vacuum terminated bulk unit cell.

A global epitaxial order parameter can then be obtained by averaging Ψ_i over all atoms at the interface. This was averaged over time for each of our simulations using reference values computed from ideal (0001), $(01\bar{1}2)$, $(10\bar{1}4)$, $(11\bar{2}6)$, $(01\bar{1}3)$, and $(01\bar{1}5)$ surfaces. The reference surface which leads to the largest global epitaxial order parameter is taken as the closest match.

IV. SIMULATION RESULTS

A summary of the simulation results and analysis is presented in Table III. Note that we ran each metadynamics simulation until the ACC slab had visibly crystallized or until the simulation reached 34 000 Gaussian bias potential depositions (corresponding to 8.3 ns). Figure 2 illustrates a typical (run 9) evolution of the six metadynamics collective variables during the crystallization portion of a metadynamics trajectory.

This article is copyrighted as indicated in the article. Reuse of AIP content is subject to the terms at: http://scitation.aip.org/termsconditions. Downloaded to IP: 144.82.108.120 On: Fri, 03 Jul 2015 13:35:29

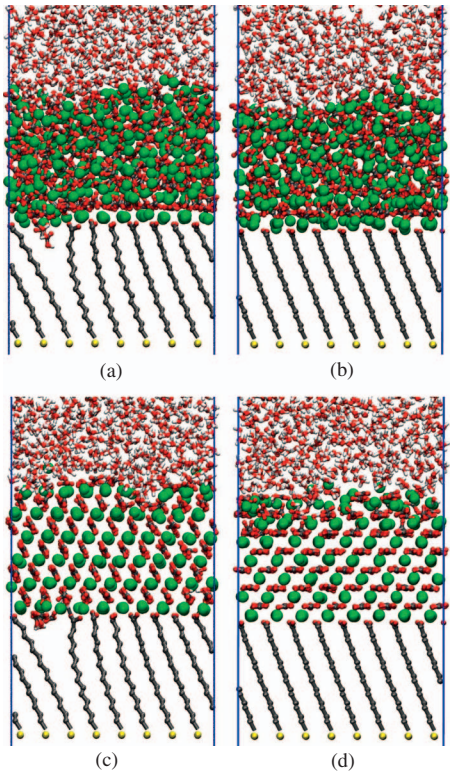

FIG. 3. Initial configurations following relaxation with MD and prior to the application of metadynamics (a) with and (b) without bicarbonate ions. The corresponding crystallized configurations following 8.3 ns of metadynamics are shown in (c) and (d). The MHA monolayers are fully ionized and kept frozen throughout the simulation.

A. Bicarbonate ions on frozen monolayers

Previously, Duffy *et al.*[22] used explicit surface energy calculations to show that the presence of bicarbonate ions at the calcite-monolayer interface acts to stabilize the $(01\bar{1}2)$ surface relative to the (0001). The role of the bicarbonate is to introduce a line defect in the SAM and hence reduce the mismatch between the array of head groups and the $(01\bar{1}2)$ calcite surface. It of interest to investigate this same influence with the current metadynamics methodology. First we examined the case of rigid MHA monolayers corresponding to simulations 1 and 2 in Table III. The initial (ACC) and final (crystallized) configurations for these two systems are shown in Fig. 3.

As can be seen from Table III the two simulations resulted in the two crystallographic orientations predicted by surface calculations, i.e., the presence of the bicarbonate defect does stabilize the $(01\bar{1}2)$ over the otherwise favored (0001) surface. This confirms the validity of the previous result and demonstrates that the thermodynamically stable crystal orientation is accessible on the crystallization timescale. Most importantly, these two crystallographic orientations have emerged naturally from the simulations and have not been imposed in constructing the calculation.

B. Odd-even effect on frozen monolayers

The above results can be contrasted against simulations 5 and 6 in which the array of frozen chains was constructed from MPA rather than MHA, and fully ionized. In common with MHA, the ideal array of carboxylate head groups has good epitaxy with the (0001) basal plane of the calcite crystal. However in this case, the introduction of line defects by reoptimizing the geometry in the presence of bicarbonate ions does not generate a superior match to an alternative face. The two simulations support this. Snapshots of the final relaxed configurations in these two simulations are shown in Fig. 4. In the ideal (no bicarbonate) case an almost perfect calcite crystal has been formed by the metadynamics, nucleated at the (0001) basal plane. Some distortion is visible in the first few crystal layers. The introduction of bicarbonate ions caused substantial disorder in the crystal at the resulting line defect, but did not alter the orientation of the crystal.

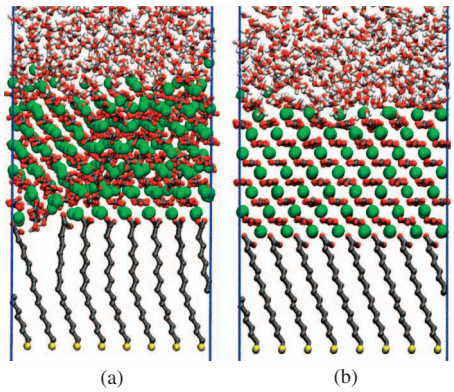

FIG. 4. Final configuration of crystallization simulations on frozen, fully ionized monolayers of MPA (a) with and (b) without the inclusion of bicarbonate ions to generate a line defect in the monolayer structure.

To our knowledge, no experiment has located crystals nucleated at the (0001) plane on MPA monolayers. It is therefore clear that in the case of odd chain lengths, the inclusion of bicarbonate ions is not sufficient to stabilize an experimentally observable crystal orientation.

C. Epitaxy on frozen monolayers

Figure 5 shows the arrangement of SAM head groups and of the first layer of calcium ions in the four fully ionized simulations.

Examination of this figure would suggest that epitaxial considerations have been largely responsible for selection of the nucleation plane. The degree to which defect-free MPA and MHA monolayers are well matched to the basal plane of calcite is striking, as is the match to the $(01\bar{1}2)$ plane on the defective MHA SAM. Although we do not see entire rows of missing Ca^{2+} ions at the interface (as predicted by previous work[15]), we do see substantial gaps in the first layer which may be partly responsible for achieving a charge-density match. Previous work by Freeman *et al.*[9] has demonstrated that nucleation can still occur despite substantial disorder in the head group arrangement. A number of head group arrays were tested with frozen disorder. In several cases the crystal nucleated at the (0001) plane. It is not clear if this orientation was a consequence of the particular choice of disordered configuration. In Secs. IV D and IV E we examine the effect

This article is copyrighted as indicated in the article. Reuse of AIP content is subject to the terms at: http://scitation.aip.org/termsconditions. Downloaded to IP: 144.82.108.120 On: Fri, 03 Jul 2015 13:35:29

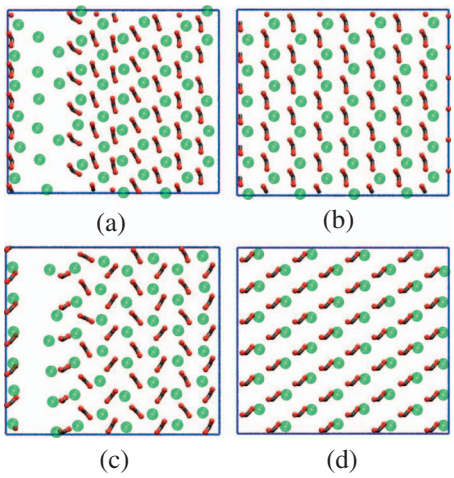

FIG. 5. Epitaxial matching between the nucleated crystal and frozen arrays of fully ionized carboxylic acid head groups. (a) MHA chains with bicarbonate-induced line defect $(01\bar{1}2)$. (b) Ideal MHA chains (0001). (c) MPA chains with bicarbonate-induced line defect (0001). (d) Ideal MPA chains (0001). In each case the head groups of the SAM are shown with oxygen atoms in red and carbon in gray. The first layer of calcium ions is shown as green spheres.

of including flexibility in the SAM and the extent to which epitaxy continues to play a role in this more realistic situation.

D. Flexibility of MHA

As indicated above, the use of metadynamics allowed simulations of crystallization to be conducted which treat the MHA monolayer dynamically. We were therefore able to investigate if this is sufficient to generate spontaneously the defects required to disrupt the epitaxy between the SAM and the (0001) face of calcite, and instead generate the experimentally observed $(01\bar{1}2)$ nucleation plane. As with the frozen monolayer, we performed simulations with fully ionized head groups, both with and without the inclusion of bicarbonate ions. These correspond to simulations 9 and 10 in Table III.

Figure 6 shows the final crystallized configuration of these two simulations. In the case of bicarbonate ions the crystal is clearly oriented in the same direction generated by the frozen MHA monolayer in Fig. 3(a). The flexibility seems to have reduced the ordering by a small degree but otherwise the result is unchanged. The defect in the monolayer associated with the presence of bicarbonate ions is no longer apparent and there is no long range positional ordering of head groups. Examination of the first layer of calcium ions indicated a region of local order at the right hand edge of the cell (away from the initial position of the bicarbonate ions) in which a good epitaxial match between the head groups and the $(01\bar{1}2)$ plane was achieved. The arrangement of head groups in this region was substantially different from that in the ideal frozen case in Fig. 5(a), suggesting a complementary nucleation process in which the head groups and calcium ions spontaneously arranged to form a nucleation site. Specifically, the monolayer is able to stimulate ordering within the nanoparticle; a partially ordered nanoparticle can then encourage the flexible monolayer to align to the crystal which in turn should encourage further ordering within the nanoparticle in a cycle of ordering from which a critical nucleus may be formed.

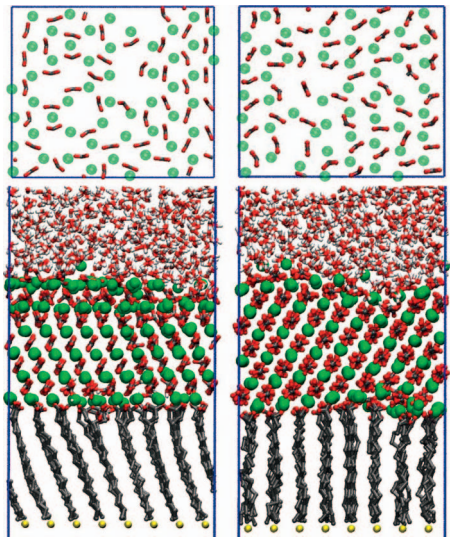

FIG. 6. Final crystallized configurations on fully ionized flexible MHA SAMs (bottom) plus arrangement of SAM head groups and first layer of calcite ions (top), both with (a) and without (b) bicarbonate ions at the calcite-monolayer interface. Although oriented differently in the *x-y* plane, both crystals have the $(01\bar{1}2)$ surface in contact with the SAM.

As with the rigid simulations, we observed missing Ca^{2+} ions at various positions in the first layer, rather than in distinct rows. Furthermore, the presence of bicarbonate ions was not required for this process to occur. Figure 6 shows the crystal exposing the $(01\bar{1}2)$ surface at the SAM interface. The surface vectors and dominant angular frequency confirm this result. Therefore without the addition of any bicarbonate or any other modification to the surface epitaxy we have induced crystallization in the experimentally observed orientation. Again there is a clearly identifiable region where the monolayer spontaneously arranged to achieve local charge-density matching (bottom right) in a fashion which bears little resemblance to its original orientation in Fig. 5(b). Table IV shows the epitaxial matching of the monolayer carbon head groups with the two relevant calcite surfaces. Clearly the surface structure of the monolayer has adjusted, losing much of its epitaxy with the (0001) surface. The matching with the $(01\bar{1}2)$ surface is also worse. Importantly the two flexible cases displayed comparable epitaxy. This suggests that global epitaxial arguments are *not* responsible for the orientational selectivity in this system when flexibility is considered.

TABLE IV. Epitaxial Order parameters for frozen and free MHA fully ionized SAMs without bicarbonates.

SAM	$01\bar{1}2$	0001
Frozen	0.46	0.96
Free	0.27	0.38

This article is copyrighted as indicated in the article. Reuse of AIP content is subject to the terms at: http://scitation.aip.org/termsconditions. Downloaded to IP: 144.82.108.120 On: Fri, 03 Jul 2015 13:35:29

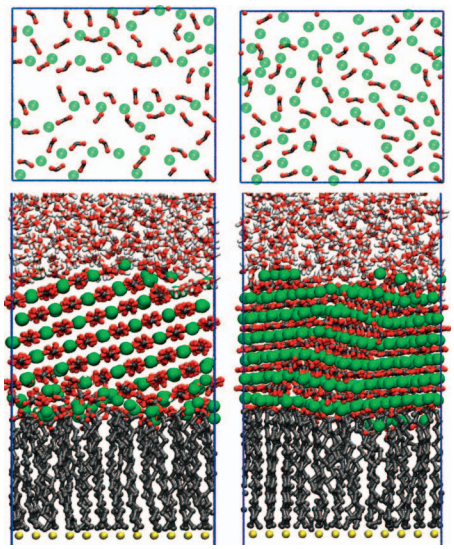

FIG. 7. Final crystallized configurations on fully ionized flexible MPA SAMs (bottom) and arrangement of SAM head groups and first layer of calcite ions (top), both with (a) and without (b) bicarbonate ions at the calcite-monolayer interface.

E. Flexibility of MPA

Snapshots showing the final crystallized configuration in simulations 13 and 14 are shown in Fig. 7. When bicarbonate ions are included crystallization produces a structure that provides a relatively good surface vector match to the $(11\bar{2}6)$ plane. Nucleation at this plane for odd chains (including MPA) has been observed as one of three major orientations in the experiments of Han and Aizenberg.[14] In this particular simulation, however, the interface between calcite and SAM is nonplanar and the arrangement of calcium ions in the first layer appears essentially random. The ordering appears to increase away from the SAM where it could alternatively be described as a stepped $(10\bar{1}4)$ surface inclined at approximately 20° to the *x*-*y* plane. Therefore crystallization may well have occurred independently of the monolayer and it is difficult to attribute this orientation to epitaxial considerations.

In the absence of bicarbonate, we observed the coexistence of two distinct crystal orientations within a single simulation. Identification of these orientations is difficult due to the presence of a large grain boundary between them, however, it was possible to identify a large region oriented with the (0001) basal plane inclined at only a slight angle to the SAM. The other orientation appears to have the $(01\bar{1}2)$ plane aligned with the SAM, and regions within the first layer of calcium ions were seen to match this plane.

In contrast with the MHA monolayers, it would appear that crystallization is far more complex on the MPA monolayers and that a variety of possible crystal planes can be selected when the monolayer is given flexibility. This is entirely consistent with the experimental observations of Han and Aizenberg in which a number of orientations were detected at this interface.

F. Ionization state

In a previous study,[9] three of the present authors established the importance of head group ionization to the control of crystallization at SAMs. Sufficient ionization is required to allow a spatial region of the monolayer to achieve charge-density matching with the selected calcite surface. Crystallization was therefore observed most easily on a fully ionized array of head groups; however, it was also possible to observe crystallization on a partially ionized array by localizing the resulting spatial distribution of charge. In the present study we have studied zero ionization, full ionization, and partial ionization with the nonionized head groups distributed *uniformly* throughout the array; it is important to note that the present model does not allow for independent proton diffusion. Inclusion of flexibility in the monolayer allows us to examine the extent to which distortions of this array are capable of generating the required local charge-density matching. In the case of frozen SAMs we therefore do not expect to see SAM-controlled crystallization on head groups with partial or zero ionization.

In all simulations with less than 100% ionization, the metadynamics simulations were halted at the maximum run length of 8.3 ns corresponding to the full 34 000 metadynamics steps. It should be stressed that the inclusion of metadynamics ensures that *all* systems will ultimately crystallize if the simulation is long enough for sufficient bias to accumulate. The observation of only partial crystallization within the same run time as the fully ionized systems is indicative of a higher free energy barrier to nucleation of the crystal phase.

1. Zero ionization

The results for non-ionized frozen monolayers are given in entries 4 and 8 of Table III. In the case of MHA monolayers the fraction of crystallized material was lower than other cases making identification of the crystal orientation somewhat difficult. For frozen MPA monolayers, simulations exhibited somewhat more crystallization. However, the slab crystallized in regions that were away from the monolayer and exposed the $(10\bar{1}4)$ surface.

Results for non-ionized flexible monolayers are given in entries 12 and 16 of Table III. For MPA monolayers the results matched the frozen case. Results for flexible MHA monolayers were more ambiguous. A crystal was formed, oriented with the $(01\bar{1}5)$ plane of the calcite crystal perpendicular to the *z* axis. This result can be reconciled by examining the structure of the SAM-calcite interface which is corrugated such that an alternating sequence of surfaces belonging to $\{10\bar{1}4\}$ was exposed to the monolayer.

In all four cases we see either poor crystallization or crystallization with $(10\bar{1}4)$ surfaces exposed. As this surface has the lowest energy in water and in vacuum, we conclude that the monolayer is exerting little or no influence on selection of crystal orientation. The data are therefore consistent with our expectations, clearly demonstrating that flexibility is not capable of generating sufficient localization of charge density to achieve a match with any polar face of calcite.

This article is copyrighted as indicated in the article. Reuse of AIP content is subject to the terms at: http://scitation.aip.org/termsconditions. Downloaded to IP: 144.82.108.120 On: Fri, 03 Jul 2015 13:35:29

2. 50% ionization

In the case of the partially charged monolayers the data are less clear. Results for MPA monolayers are given in entries 7 and 15 of Table III. Crystallization can be observed at the interface only, adopting the (0001) plane for both flexible and frozen monolayers. Only a small percentage of ions match calcite in the bulk. This is similar to observations in vacuum simulations[9] where partially ionized monolayers were unable to induce crystallization of the whole particle, suggesting that flexibility of the monolayer alone cannot overcome the unfavorable distribution of charge. In experiments an alternative mechanism may be migration of protons to form a concentration of ionized head groups. Deprotonation events and hence migration of effective charge across molecules are not modeled in our simulations and this mechanism is not accessible. The complementary nucleation process exemplified by the ionized MHA is hence unable to operate.

Results for partially ionized MHA monolayers are given as entries 3 and 11 in Table III. When the monolayer is frozen a small degree of crystallization was observed at the interface. The resulting plane was uncertain but most closely matches $(01\bar{1}5)$. For the flexible monolayer crystallization was again limited. In common with the nonionized case the crystal is *oriented* perpendicular to $(01\bar{1}5)$ but exposes a series of $(10\bar{1}4)$ surfaces to the monolayer.

We can therefore conclude that flexibility of the monolayer is not in itself sufficient to reduce the ionization requirement for observing crystallization in simulations. We suggest that in experiments, the complementary nucleation of head group and calcium ion order is accompanied by a nucleation of charge density, i.e., a spatial concentration of ionized head groups. Observing this effect in simulations would require a reactive force field to model the formation and breaking of O–H bonds as protons migrate away from the nucleation site.

G. Solvent effects

By contrasting our simulations with the previous vacuum studies, we can examine the influence of the solvent. For both the fully ionized MHA and MPA cases the frozen monolayers produced (0001) calcite, as observed in the vacuum simulations. For the partially ionized simulations we also observe a small amount of (0001) calcite at the interface. In the case of zero ionization no crystallization was observed for the vacuum simulations. As noted above, the inclusion of metadynamics will ultimately generate crystallization in any system independently of the monolayer. Our results suggest that this manifests by crystallization away from the interface and exposing $(10\bar{1}4)$ in cases where the monolayer plays no role. This result should therefore be taken as equivalent to "no crystallization" in the vacuum study and hence the two sets of results are entirely consistent. This suggests that the solvent-calcite interface is exerting little influence in controlling crystallization.

V. CONCLUSIONS

We have performed a series of simulations for calcium carbonate in an aqueous environment in contact with two different SAMs, MHA and MPA. By employing the metadynamics method, we have been able to observe crystallization of a calcium carbonate nanoparticle under physically realistic conditions, inaccessible to standard MD.

By varying the ionization of the monolayer we explored its influence on crystallization. Our results indicated that ionization is essential to induce crystallization in the particle. When the monolayer was partially ionized crystallization was always extremely limited or took place away from the interface. Adding flexibility to the monolayer did not allow the system to adjust for this drop in surface charge by, for example, creating the correct surface charge density in small regions. It is interesting to consider where the cutoff might exist for the necessary degree of surface ionization needed to crystallize the whole deposit. At standard *p*H, however, we argue that regions of fully ionized head groups as large as (if not larger) than our simulated cell are likely to exist.

The role of flexibility of the monolayer has been discussed in the literature in some detail, and our simulations demonstrated it can aid the selectivity of the film. Despite superior epitaxial matching between the MHA head groups and the (0001) surface, when the monolayer was allowed to move crystallization produced the experimentally observed $(01\bar{1}2)$. Previous simulations have demonstrated that this is only energetically favorable with the introduction of bicarbonate to disrupt the monolayer order or by restricting the crystal growth to the direction that is largely commensurate between the monolayer and $(01\bar{1}2)$ surface. We have now demonstrated that the monolayer is able to adjust its structure to better match the growing crystal and that a structural feedback between the crystal and monolayer exists. This suggests that structural analysis of a monolayer in contact with a particular crystal surface should show a greater matching between the surface vectors than might be expected, as the monolayer will adjust to match the crystal.

We suggest that the current methodology could be applied to a range of similar systems and has the potential to yield valuable insight as a general tool in the computational study of biomineralization.

ACKNOWLEDGMENTS

The authors wish to acknowledge the support of the EPSRC through Grant Nos. GR/S80127 and GR/S80103. Some calculations were performed using the HECToR supercomputing facility under EPSRC Grant No. EP/F055471/1. The use of facilities at the University of Warwick Centre for Scientific Computing is also gratefully acknowledged.

[1] E. DiMasi, S.-Y. Kwak, F. Amos, M. Olszta, D. Lush, and L. Gower, Phys. Rev. Lett. **97**, 045503 (2006).
[2] R. S. K. Lam, J. M. Charnock, A. Lennie, and F. C. Meldrum, Cryst. Eng. Comm **9**, 1226 (2007).
[3] N. A. J. M. Sommerdijk and G. de With, Chem. Rev. (Washington, D.C.) **108**, 4499 (2008).
[4] D. Duffy and J. Harding, Langmuir **20**, 7630 (2004).
[5] B. P. Pichon, P. H. H. Bomans, P. M. Frederik, and N. A. J. M. Sommer-

This article is copyrighted as indicated in the article. Reuse of AIP content is subject to the terms at: http://scitation.aip.org/termsconditions. Downloaded to IP: 144.82.108.120 On: Fri, 03 Jul 2015 13:35:29

dijk, J. Am. Chem. Soc. **130**, 4034 (2008).
[6] Y. Chen, J. Xiao, Z. Wang, and S. Yang, Langmuir **25**, 1054 (2009).
[7] D. Quigley and P. M. Rodger, J. Chem. Phys. **128**, 221101 (2008).
[8] D. Duffy and J. Harding, Surf. Sci. **595**, 151 (2005).
[9] C. L. Freeman, J. H. Harding, and D. M. Duffy, Langmuir **24**, 9607 (2008).
[10] J. Aizenberg, A. Black, and G. Whitesides, J. Am. Chem. Soc. **121**, 4500 (1999).
[11] A. Travaille, J. Donners, J. Gerritsen, N. Sommerdijk, R. Nolte, and H. van Kempen, Adv. Mater. (Weinheim, Ger.) **14**, 492 (2002).
[12] A. Travaille, L. Kaptijn, P. Verwer, B. Hulsken, J. Elemans, R. Nolte, and H. van Kempen, J. Am. Chem. Soc. **125**, 11571 (2003).
[13] J. D. H. Donnay and D. Harker, Am. Mineral. **22**, 446 (1937).
[14] Y. Han and J. Aizenberg, Angew. Chem., Int. Ed. **42**, 3668 (2003).
[15] D. Duffy and J. Harding, Langmuir **20**, 7637 (2004).
[16] C. L. Freeman, J. H. Harding, D. J. Cooke, J. A. Elliott, J. S. Lardge, and D. M. Duffy, J. Phys. Chem. C **111**, 11943 (2007).
[17] A. Pavese, M. Catti, G. D. Price, and R. A. Jackson, Phys. Chem. Miner. **19**, 80 (1992).
[18] A. Pavese, M. Catti, S. C. Parker, and A. Wall, Phys. Chem. Miner. **23**, 89 (1996).
[19] W. L. Jorgensen, J. Chandrasekhar, J. Madura, R. W. Impey, and M. L. Klein, J. Chem. Phys. **79**, 926 (1983).
[20] A. MacKerell, D. Bashford, M. Bellott, R. Dunbrack, J. Evanseck, M. Field, S. Fischer, J. Gao, H. Guo, S. Ha, D. Joseph-McCarthy, L. Kuchnir, K. Kuczera, F. T. K. Lau, C. Mattos, S. Michnick, T. Ngo, D. T. Nguyen, B. Prodhom, W. E. Reiher III, B. Roux, M. Schlenkrich, J. C. Smith, R. Stote, J. Straub, M. Watanabe, J. Wiórkiewicz-Kuczera, D. Yin, and M. Karplus, J. Phys. Chem. B **102**, 3586 (1998).
[21] A. MacKerel, Jr., C. Brooks III, L. Nilsson, B. Roux, Y. Won, and M. Karplus, *CHARMM: The Energy Function and Its Parameterization with an Overview of the Program*, The Encyclopedia of Computational Chemistry Vol. 1 (Wiley, Chichester, 1998), pp. 271–277.
[22] D. M. Duffy, A. M. Travaille, H. van Kempen, and J. H. Harding, J. Phys. Chem. B **109**, 5713 (2005).
[23] D. Duffy and J. Harding, Langmuir **21**, 3850 (2005).
[24] W. Smith, T. R. Forester, and I. T. Todorov, DL_POLY, a molecular dynamics simulation package, STFC's Daresbury Laboratory via the Web site http://www.ccp5.ac.uk/DL_POLY.
[25] D. Quigley (unpublished).
[26] W. G. Hoover, Phys. Rev. A **31**, 1695 (1985).
[27] A. Laio and M. Parrinello, Proc. Natl. Acad. Sci. U.S.A. **99**, 12562 (2002).
[28] D. Quigley and P. M. Rodger, Mol. Simul. **35**, 613 (2009).
[29] A. Laio and F. L. Gervasio, Rep. Prog. Phys. **71**, 126601 (2008).
[30] N. H. de Leeuw and S. C. Parker, J. Phys. Chem. B **102**, 2914 (1998).
[31] D. Duffy and J. Harding, J. Mater. Chem. **12**, 3419 (2002).
[32] J. R. Morris, Phys. Rev. B **66**, 144104 (2002).

This article is copyrighted as indicated in the article. Reuse of AIP content is subject to the terms at: http://scitation.aip.org/termsconditions. Downloaded to IP: 144.82.108.120 On: Fri, 03 Jul 2015 13:35:29